

## Supporting Information

for

**Promoted photocarriers transfer and increased active sites for optimal CO<sub>2</sub>-to-CH<sub>4</sub> photoconversion via the modification of atomically dispersed transition metal ions in CdZnS nanocrystals**

Hai-Bo Huang,<sup>a,b,c</sup> Hui-Ying Zhang,<sup>a</sup> Feng-Ying Cai,<sup>a</sup> Ya-Feng Li,<sup>d</sup> Jian Lü,<sup>\*a,b,d</sup> and Rong Cao<sup>b,c</sup>

<sup>a</sup>Fujian Provincial Key Laboratory of Soil Environmental Health and Regulation, College of Resources and Environment, Fujian Agriculture and Forestry University, Fuzhou 350002, P.R. China;

<sup>b</sup>State Key Laboratory of Structural Chemistry, Fujian Institute of Research on the Structure of Matter, Chinese Academy of Sciences, Fuzhou 350002, P.R. China; <sup>c</sup>University of Chinese Academy

of Sciences, Beijing 100049, P.R. China; <sup>d</sup>State Key Laboratory of Photocatalysis on Energy and Environment, Fuzhou University, No. 2 Xue Yuan Road, Fuzhou 350116, China.

\*Corresponding author. E-mail: jian\_lu\_fafu@163.com.

*Number of pages: 14*

*Number of tables: 1*

*Number of figures: 10*

## Experimental

**Materials.** Cadmium acetate ( $\text{Cd}(\text{Ac})_2 \cdot 2\text{H}_2\text{O}$ ), zinc acetate ( $\text{Zn}(\text{Ac})_2 \cdot 2\text{H}_2\text{O}$ ), cobalt acetate ( $\text{Co}(\text{Ac})_2 \cdot 4\text{H}_2\text{O}$ ), copper acetate ( $\text{Cu}(\text{Ac})_2 \cdot \text{H}_2\text{O}$ ), nickelous acetate ( $\text{Ni}(\text{Ac})_2 \cdot 4\text{H}_2\text{O}$ ) and sodium sulfide ( $\text{Na}_2\text{S} \cdot 9\text{H}_2\text{O}$ ) were of analytical reagent grade and used as received. Reaction and stock solutions were prepared by using deionized ultrapure water.

**Preparation of CZS- $\text{M}^{2+}$  (M = Co/Cu/Ni) nanocrystals.** The CZS- $\text{M}^{2+}$  materials were synthesized via a simple hydrothermal method using deionized water as the solvent. In a typical synthesis for CZS- $\text{Cu}^{2+}$ , 2.5 mmol  $\text{Cd}(\text{Ac})_2 \cdot 2\text{H}_2\text{O}$ , 2.2 mmol  $\text{Zn}(\text{Ac})_2 \cdot 2\text{H}_2\text{O}$ , 0.3 mmol  $\text{Cu}(\text{Ac})_2 \cdot \text{H}_2\text{O}$  and 5.0 mmol  $\text{Na}_2\text{S} \cdot 9\text{H}_2\text{O}$  were mixed in 20 mL distilled water under magnetic stirring for 1 h. The resultant brown mixture was then transferred into a 50 mL Teflon-lined autoclave and maintained at 160 °C for 12 h in oven. Finally, the precipitates were obtained by centrifugation and washed three times with deionized water and ethanol, respectively, dried at 70 °C for 6 h and named as CZS- $\text{Cu}^{2+}$ . For the synthesis of CZS- $\text{M}^{2+}$ , various metal acetates were used in replacement of  $\text{Cu}(\text{Ac})_2 \cdot \text{H}_2\text{O}$  by following the above described procedure. In addition, as-prepared CZS- $\text{M}^{2+}$  (M = Co/Cu/Ni) nanocrystals were heated in tubular furnace at 300 °C for 2 h under mixed  $\text{H}_2/\text{N}_2$  (5%/95%) to remove impurities at surfaces.

**Evaluation of photocatalytic activity.** In a typical process, 5.0 mg of powder photocatalyst dispersed in 1.0 mL of deionized water was immobilized onto a  $\phi 34$  mm quartz filter membrane (Fig.S6; ESI), and then the water solvent was evaporated with the irradiation of an infrared lamp. The photocatalyst-loaded membrane was moved into a 250 mL photoreactor with 3.0 mL of aqueous solution and suspended on the top of the reactor. Prior to illumination, the reactor was vacuumed and subsequently backfilled with ultra-pure  $\text{CO}_2$  (99.999%) for about 1 h to reach the

adsorption/desorption equilibrium of CO<sub>2</sub> at the surface of photocatalyst. The pressure of the reactor was maintained at 60 kPa and temperature was kept at 4 °C using circulating water. The visible-light irradiation was provided by a light-intensity-controlled xenon lamp (PLS-SXE300D, Beijing, PerfectLight) equipped with a UV-cut filter ( $\lambda \geq 420$  nm), while the simulated solar irradiation (UV-vis-NIR) was acquired by the same lamp with a full-range reflector and an AM 1.5 G filter. The lamp was about 7.5 cm away from the catalyst membrane and the irradiance intensity was measured by a light power meter (PL-MW2000, Beijing, PerfectLight). Photocatalytic reactions were performed for 10 h at 4 °C, and the gaseous products were analyzed online every hour by using an Agilent GC7820 gas chromatograph equipped with two tandem chromatographic columns (Porapak Q and 5A Molecular sieve), an FID detector and a TCD detector. During the durability test, the reaction system was evacuated every 10 h and refilled with ultra-pure CO<sub>2</sub> and water.

### **Characterizations**

Powder X-ray diffraction (PXRD) patterns were collected using a Rigaku Miniflex 600 X-ray diffractometer with Cu K $\alpha$  radiation ( $\lambda = 0.154$  nm). Scanning electron microscopy (SEM) images were photographed by using a JSM6700-F with a working voltage of 10 kV. Transmission electron microscopy (TEM) and high-resolution TEM (HR-TEM) images were recorded by using an FEIT 20 working at 200 kV. The inter-planer distances and the inverse Fast Fourier Transform (FFT) were calculated using the Digital Micrograph software. X-ray photoelectron spectroscopy (XPS) measurements were performed on a Thermo Fisher ESCALAB 250Xi spectrometer with Al K $\alpha$  X-ray source (15 kV, 10 mA). In order to compensate effects related to charge shifts C 1s peak at 284.6 eV was used as internal standard. Diffuse reflectance spectra (DRS) were recorded on a Shimadzu UV-vis spectrophotometer (UV-2550) with BaSO<sub>4</sub> as the background. The

photoluminescence (PL) spectra and time-resolved fluorescence emission spectrum were collected on a FLS 980 fluorometer spectrometer at room temperature. Electron spin resonance (ESR) spectra were recorded on a Bruker E500 spectrometer.

### **Photoelectrochemical tests**

The photoelectrochemical test was performed on an electrochemical analyzer (Zahner, Germany) in a standard three-electrode cell. The  $\text{Na}_2\text{SO}_4$  (0.2 M, pH = 6.8) aqueous solution was used as supporting electrolyte. The suspension of samples was prepared by mixing 5 mg of catalysts with 1 mL ethanol and 50  $\mu\text{L}$  Nafion and then sonication for 1 h. The catalyst-coated indium tin oxide (ITO) glass (1  $\text{cm}^2$  in deposition area) was used to be the working electrode. The counter and reference electrodes were Pt mesh and Ag/AgCl, respectively [S1, S2]. The transient photocurrent measurements were recorded under the visible light illumination and a 300-W Xe lamp equipped with an optical cutoff filter of 420 nm was employed for the visible-light excitation. Electrochemical impedance spectroscopy (EIS) plots were collected at off circuit potentials, with the frequency ranging from 100 kHz to 0.1 Hz and modulation amplitude of 5 mV. Mott-Schottky curves were recorded in dark with a voltage of 5 mV at frequencies of 1.0 kHz, respectively [S3].

### **Computational details**

All the density functional theory (DFT) calculations in this work were performed using the Vienna ab-initio simulation package (VASP) [S4–S7]. The projector augmented wave (PAW) approach was used to describe the interactions between ion cores and valence electrons [S8]. The generalized gradient approximation with the Perdew–Burke–Ernzerhof exchange correlation functional (GGA–PBE) was employed to describe the exchange–correlation functional [S9, S10]. The Kohn–Sham equations was expanded in a plane wave basis set with a cutoff energy of 400 eV.

The Brillouin zone integration was accomplished using  $3\times 3\times 1$  Monkhorst–Pack k–point grid [S11]. To illustrate the long–range dispersion interactions between the adsorbates and catalysts, the D3 correction method of Grimme was employed. The  $3\times 3$  supercell of CZS (110) and Cu atom doped CZS (110) surfaces with four atomic layers were chosen to construct the investigated periodic slab models. During optimization, the top two layers were relaxed and the bottom two layers were fixed.

## References

- [S1] H. B. Huang, Y. Wang, W. B. Jiao, F. Y. Cai, M. Shen, S. G. Zhou, H. L. Cao, J. Lü and R. Cao, *ACS Sustain. Chem. Eng.*, 2018, **6**, 7871–7879.
- [S2] X. Q. Hao, J. Zhou, Z. W. Cui, Y. C. Wang, Y. Wang and Z. G. Zou, *Appl. Catal. B–Environ.*, 2018, **229**, 41–51.
- [S3] H. Liu, C. Y. Xu, D. D. Li and H. L. Jiang, *Angew. Chem. Int. Ed.*, 2018, **57**, 5379–5383.
- [S4] G. Kresse, J. Hafner, *Phys. Rev. B*, 1993, **47**, 558–561.
- [S5] G. Kresse, J. Hafner, *Phys. Rev. B*, 1994, **49**, 14251–14269.
- [S6] G. Kresse, J. Furthmüller, *Comp. Mater. Sci.*, 1996, **6**, 15–50.
- [S7] G. Kresse, J. Furthmüller, *Phys. Rev. B*, 1996, **54**, 11169–11186.
- [S8] P. E. Blöchl, *Phys. Rev. B*, 1994, **50**, 17953–17979.
- [S9] G. Kresse, D. Joubert, *Phys. Rev. B*, 1999, **59**, 1758–1775.
- [S10] J. P. Perdew, K. Burke, *Phys. Rev. Lett.*, 1996, **77**, 3865–3868.
- [S11] H. J. Monkhorst, J. D. Pack, *Phys. Rev. B*, 1976, **13**, 5188–5192.

**Table. S1** Comparison of CO<sub>2</sub> photoreduction capacity over various photocatalysts under different conditions.

Catalyst	Light source	Experimental condition	Production rate ( $\mu\text{mol h}^{-1} \text{g}^{-1}$ )	Reference
CdS–WO <sub>3</sub>	300 W (Xe) ( $\lambda \geq 420$ nm)	CO <sub>2</sub> and H <sub>2</sub> O vapor	1.02	S12
RGO–CdS	300 W (Xe) ( $\lambda \geq 420$ nm)	CO <sub>2</sub> and H <sub>2</sub> O vapor	2.51	S13
Au–MoS <sub>2</sub>	300 W (Xe)	CO <sub>2</sub> and H <sub>2</sub> O	13.98	S14
3D–SiC@2D–MoS <sub>2</sub>	300 W (Xe) ( $\lambda \geq 420$ nm)	CO <sub>2</sub> and H <sub>2</sub> O vapor	14.41	S15
ZnIn <sub>2</sub> S <sub>4</sub> /TiO <sub>2</sub>	AM 1.5 G; 300 W (Xe)	CO <sub>2</sub> and H <sub>2</sub> O vapor	1.13	S16
S–vacancy CuIn <sub>5</sub> S <sub>8</sub>	300 W (Xe) with AM 1.5 filter and a 420 nm cutoff filter	CO <sub>2</sub> and H <sub>2</sub> O vapor	8.7	S17
Co–doped MgIn <sub>2</sub> S <sub>4</sub>	300 W (Xe) ( $\lambda \geq 420$ nm)	CO <sub>2</sub> and H <sub>2</sub> O vapor	1.60	S18
Bi <sub>2</sub> S <sub>3</sub> /UiO–66	UV–vis light	CO <sub>2</sub> and H <sub>2</sub> O vapor	0.31	S19
Bi <sub>2</sub> S <sub>3</sub> /MoS <sub>2</sub>	Visible light	CO <sub>2</sub> and H <sub>2</sub> O	0.25	S20
<b>CZS–Cu<sup>2+</sup></b>	<b>300 W (Xe) <math>\lambda \geq 420</math> nm</b>	<b>CO<sub>2</sub> and H<sub>2</sub>O vapor</b>	<b>29.72</b>	<b>This work</b>

## References

- [S12] J. Jin, J. Yu, D. Guo, C. Cui and W. Ho, *Small*, 2015, **11**, 5262–5271.
- [S13] J. Yu, J. Jin, B. Cheng and M. Jaroniec, *J. Mater. Chem. A*, 2014, **2**, 3407–3416.
- [S14] S. Sun, Q. An, M. Watanabe, J. Cheng, H. H. Kim, T. Akbay, A. Takagaki and T. Ishihara, *Appl. Catal. B–Environ.*, 2020, **271**, 118931.
- [S15] Y. Wang, Z. Zhang, L. Zhang, Z. Luo, J. Shen, H. Lin, J. Long, J. C. S. Wu, X. Fu, X. Wang and C. Li, *J. Am. Chem. Soc.*, 2018, **140**, 14595–14598.
- [S16] G. Yang, D. Chen, H. Ding, J. Feng, J. Z. Zhang, Y. Zhu, S. Hamid and D. W. Bahnemann, *Appl. Catal. B–Environ.*, 2017, **219**, 611–618.
- [S17] X. Li, Y. Sun, J. Xu, Y. Shao, J. Wu, X. Xu, Y. Pan, H. Ju, J. Zhu and Y. Xie, *Nat. Energy*, 2019, **4**, 690–699.
- [S18] C. Zeng, Q. Zeng, C. Dai and Y. Hu, *Dalton Trans.*, 2020, **49**, 9213–9217.
- [S19] X. Chen, Q. Li, J. Li, J. Chen and H. Jia, *Appl. Catal. B–Environ.*, 2020, **270**, 118915.
- [S20] R. Kim, J. Kim, J. Y. Do, M. W. Seo and M. Kang, *Catalysts*, 2019, **9**, 998.

## Figure Caption

**Fig. S1.** PXRD patterns of (a) CZS–M (M = Co/Cu/Ni); and (b) CZS–Cu and CZS–Cu<sup>2+</sup>.

**Fig. S2.** XPS survey spectra of CZS and CZS–M<sup>2+</sup>.

**Fig. S3.** High-resolution XPS spectra of (a–b) CZS–Cu and CZS–Cu<sup>2+</sup>; (c) CZS–Co and CZS–Co<sup>2+</sup>; and (d) CZS–Ni and CZS–Ni<sup>2+</sup>.

**Fig. S4.** (a) Photocatalytic CO<sub>2</sub> reduction performance; and (b) production selectivity of CZS–M.

**Fig. S5.** (a) Photocatalytic CO<sub>2</sub> reduction of CZS–Cu<sup>2+</sup> for a series of control experiments; (b) wavelength-dependent AQY of CO<sub>2</sub> photoreduction to CH<sub>4</sub> over CZS–Cu<sup>2+</sup>; (c) high-resolution XPS spectra of Cu 2p for the CZS–Cu<sup>2+</sup> before and after CO<sub>2</sub> photoreduction; and (d) in-situ diffuse reflectance infrared Fourier transform spectroscopy (DRIFTS) for CZS–Cu<sup>2+</sup> in the CO<sub>2</sub> and H<sub>2</sub>O vapor under visible irradiation.

**Fig. S6.** Samples on  $\phi$ 34 mm quartz filter membrane before (fresh) and after (used) photocatalytic experiments.

**Fig. S7.** (a) Transient photocurrent; and (b) EIS Nyquist plots of CZS–Cu and CZS–Cu<sup>2+</sup>.

**Fig. S8.** Structural models optimized by various reaction intermediates of CZS (a) and CZS–Cu<sup>2+</sup> (b).

**Fig. S9.** The binding Energy of (a) \*CO; and (b) \*H of CZS (110) and CZS–Cu<sup>2+</sup> (110).

**Fig. S10.** (a) Slice of surface charge distribution diagram of perfect and Cu<sup>2+</sup>-doped CZS; (b) the charge density difference maps of CZS–Cu<sup>2+</sup> (110) surface (yellow region represents the electron accumulation, blue region represents the electron deletion, Isosurfaces = 0.001 e/bohr<sup>3</sup>).

Fig. S1

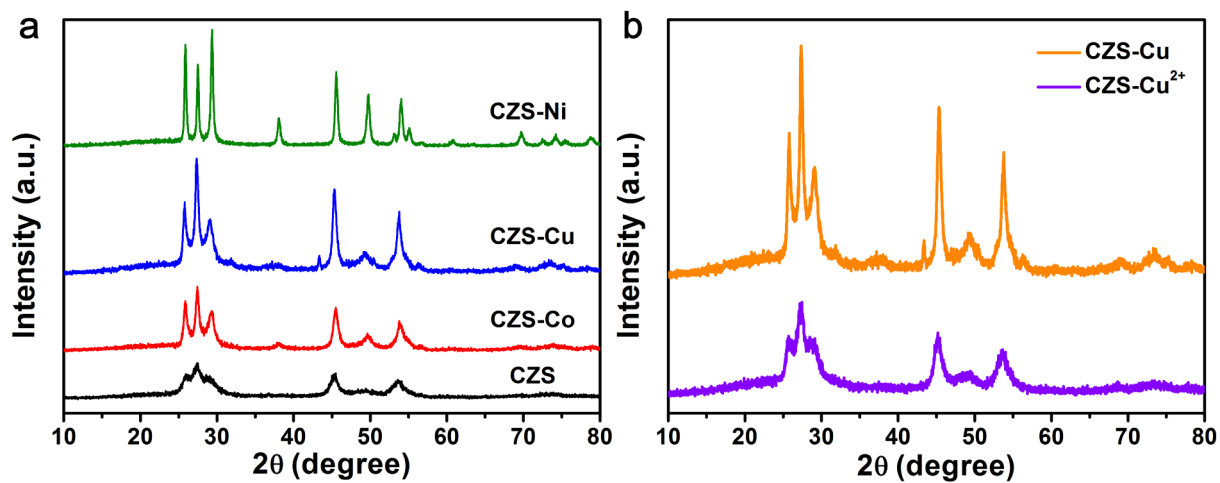


Fig. S2

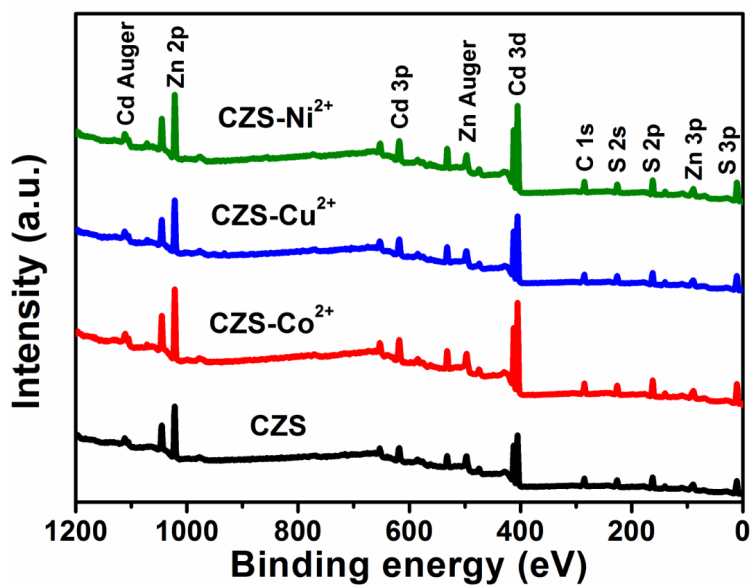


Fig. S3

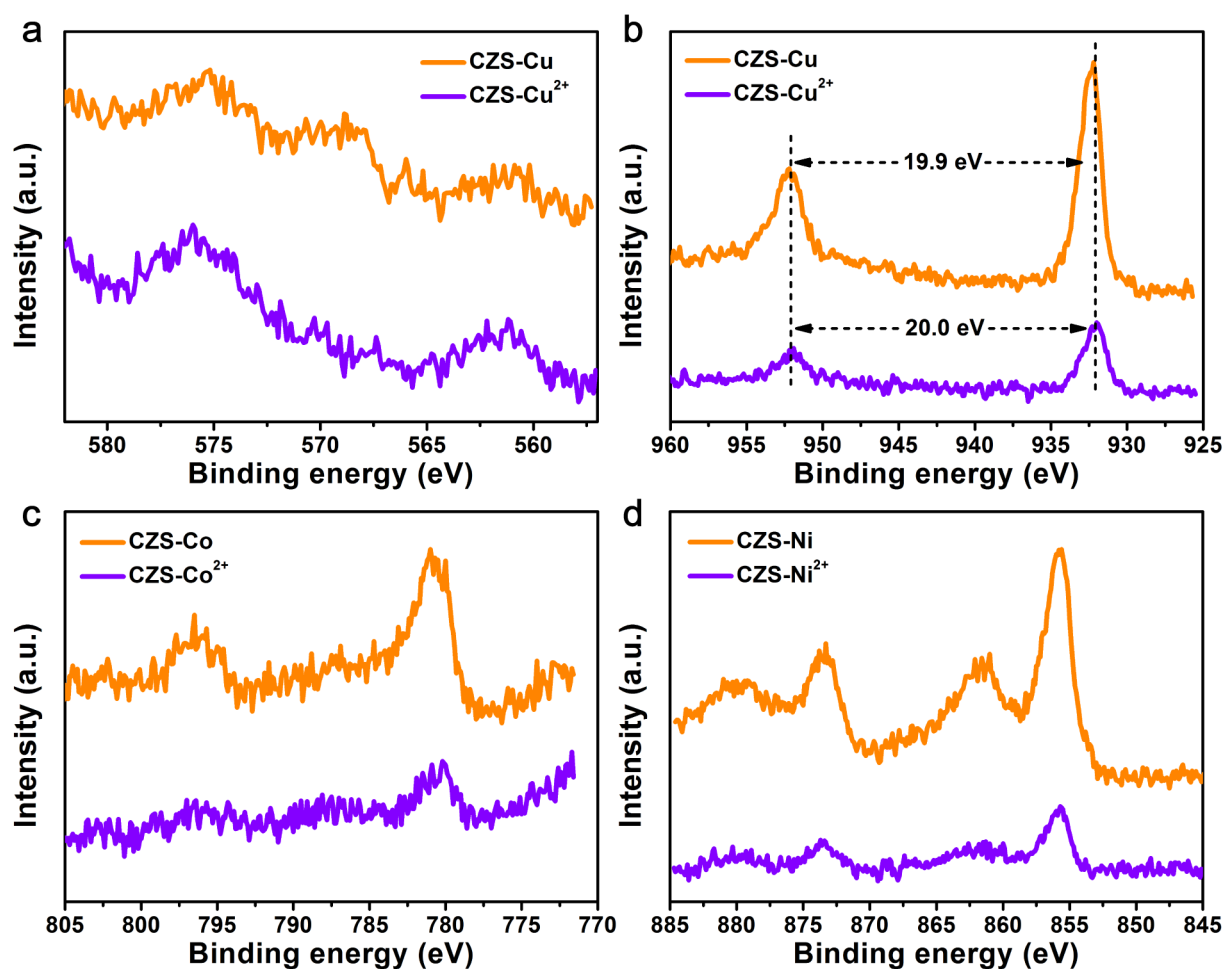


Fig. S4

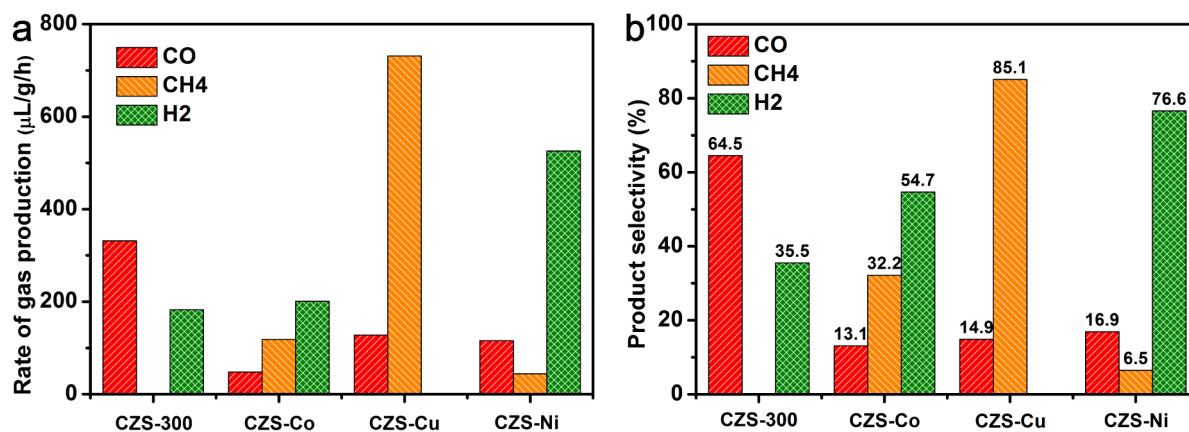


Fig. S5

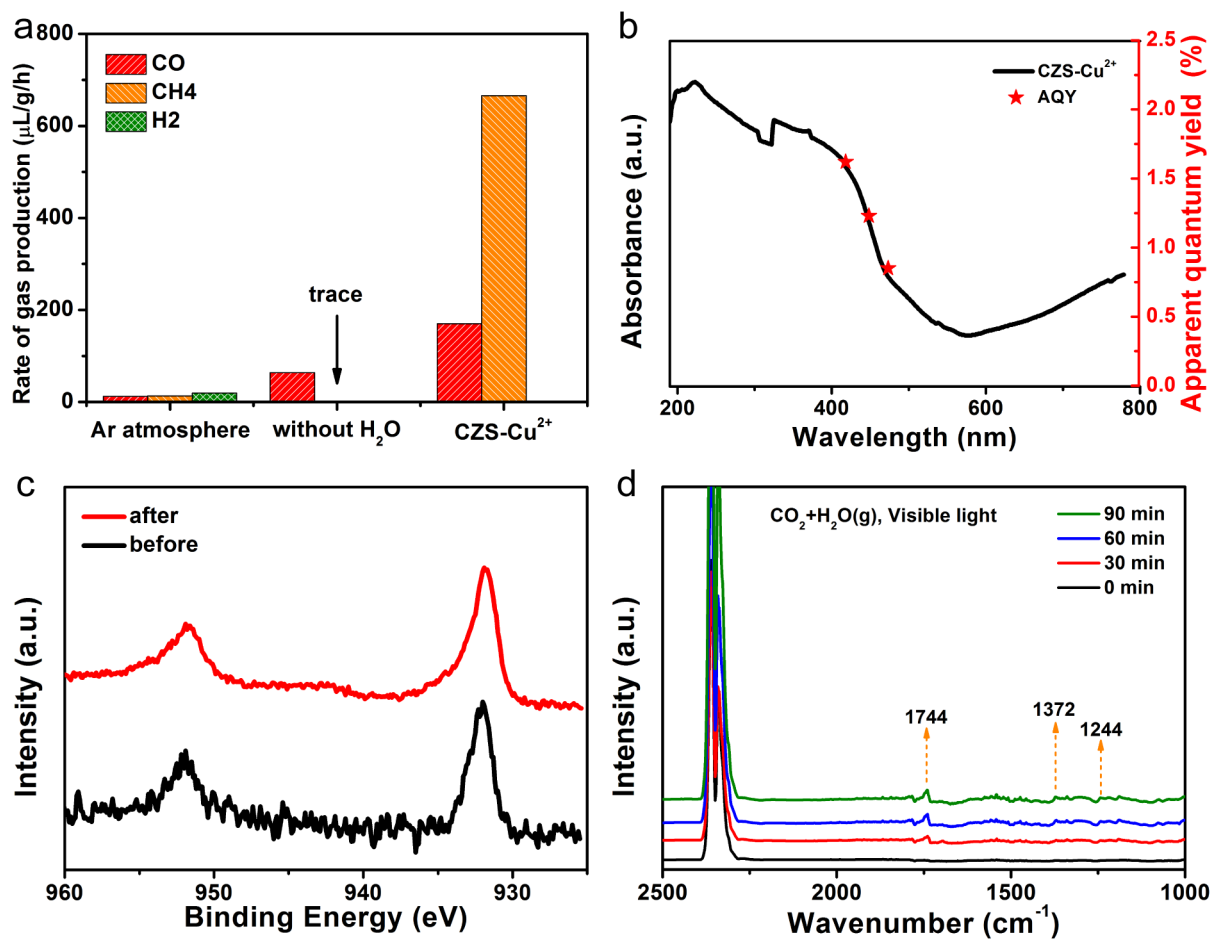


Fig. S6

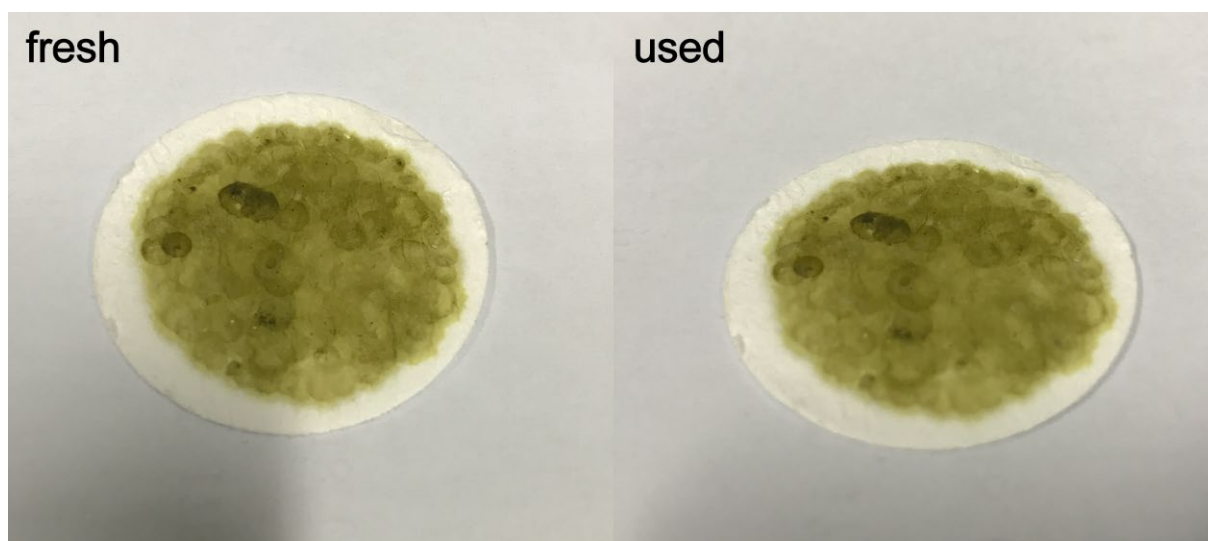


Fig. S7

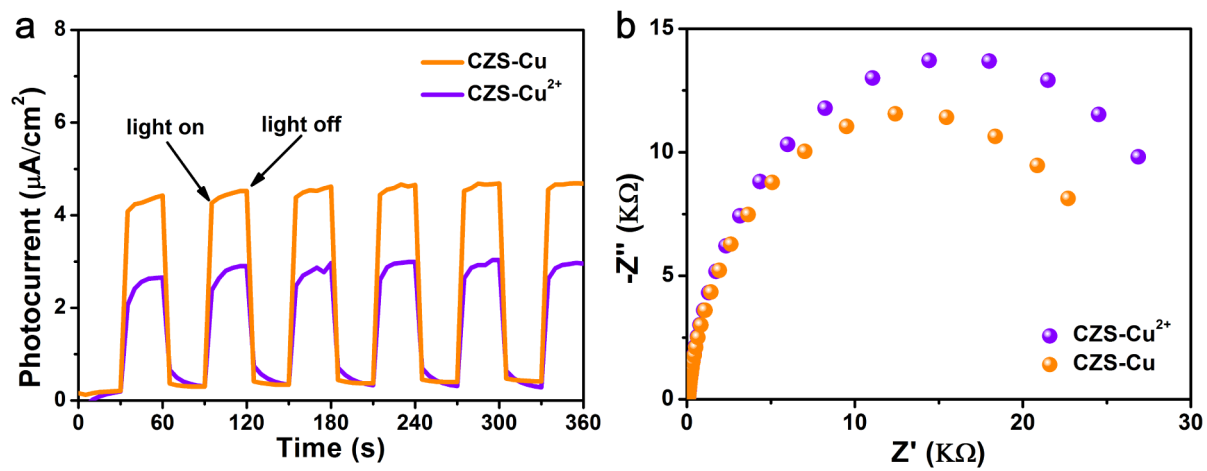


Fig. S8

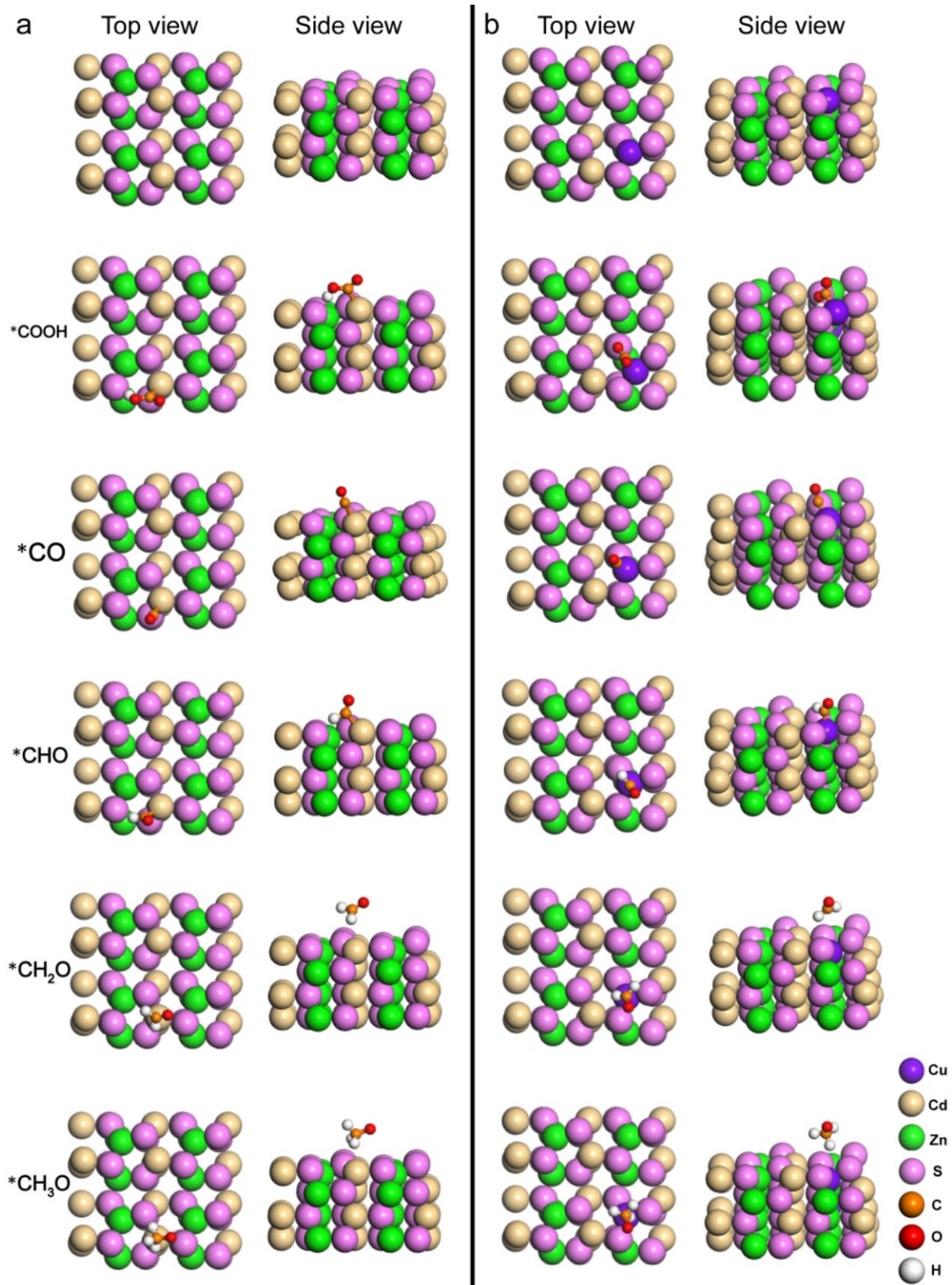


Fig. S9

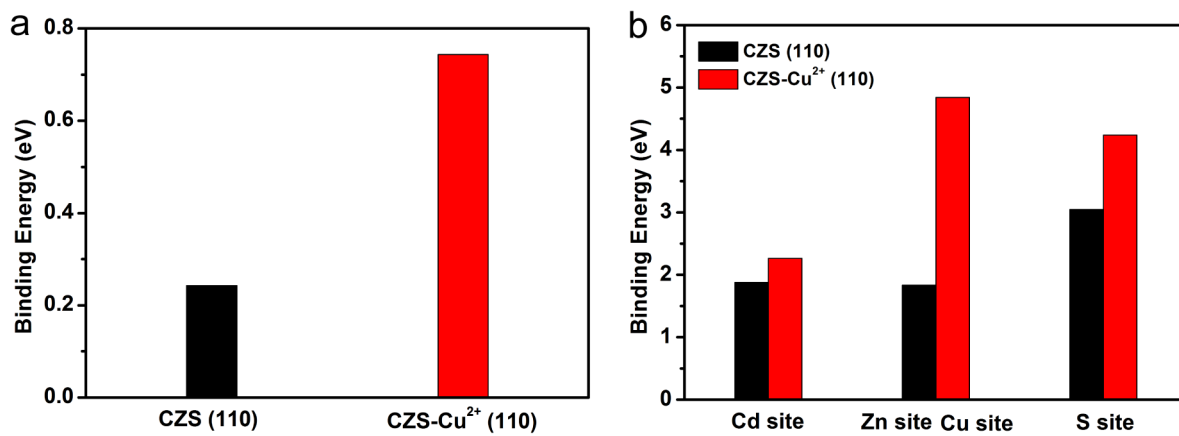


Fig. S10

